

# Longitudinal and transversal spin dynamics of donor-bound electrons in fluorine-doped ZnSe: spin inertia versus Hanle effect

F. Heisterkamp<sup>1</sup>, E. A. Zhukov<sup>1</sup>, A. Greulich<sup>1</sup>, D. R. Yakovlev<sup>1,2</sup>, V. L. Korenev<sup>1,2</sup>, A. Pawlis<sup>3,4</sup> and M. Bayer<sup>1,2</sup>

<sup>1</sup>*Experimentelle Physik 2, Technische Universität Dortmund, 44221 Dortmund, Germany*

<sup>2</sup>*Ioffe Physical-Technical Institute, Russian Academy of Sciences, 194021 St. Petersburg, Russia*

<sup>3</sup>*Peter Grünberg Institute, Forschungszentrum Jülich, 52425 Jülich, Germany and*

<sup>4</sup>*Department Physik, Universität Paderborn, 33098 Paderborn, Germany*

(Dated: August 13, 2018)

The spin dynamics of the strongly localized, donor-bound electrons in fluorine-doped ZnSe epilayers is studied by pump-probe Kerr rotation techniques. A method exploiting the spin inertia is developed and used to measure the longitudinal spin relaxation time,  $T_1$ , in a wide range of magnetic fields, temperatures, and pump densities. The  $T_1$  time of the donor-bound electron spin of about 1.6  $\mu$ s remains nearly constant for external magnetic fields varied from zero up to 2.5 T (Faraday geometry) and in a temperature range 1.8 – 45 K. The inhomogeneous spin dephasing time,  $T_2^* = 8 - 33$  ns, is measured using the resonant spin amplification and Hanle effects under pulsed and steady-state pumping, respectively. These findings impose severe restrictions on possible spin relaxation mechanisms.

PACS numbers: 72.25.Rb, 71.55.Gs, 61.72.uj, 71.70.Ej

## I. INTRODUCTION

Recently the coherent dynamics of spin excitations in semiconductor heterostructures has attracted considerable interest, motivated in particular by the observation of long electron spin relaxation and coherence times [1], one of the main prerequisites for a system to be suited for quantum information technologies. To obtain access to these times, optical techniques have proved to be an effective measurement tool.

Generally, the phenomenon of optical orientation is used to create the initial spin orientation [2]. It involves two processes: the photogeneration of spin-oriented carriers by absorption of circularly polarized light and the possible spin relaxation with the characteristic time  $\tau_S$  during the lifetime  $\tau$  of these carriers [2]. In order to determine absolute values of these times one often uses an “internal clock” of the system: The periodic Larmor precession of the electron spins about an external magnetic field with the frequency  $\Omega_L = \mu_B g_e B / \hbar$  can be used as such a clock. Here  $\mu_B$  is the Bohr magneton and  $g_e$  is the Landé factor of the electrons. One of the common methods to study spin lifetimes  $T_S = 1/(1/\tau + 1/\tau_S)$  in atoms [3, 4] and in solid state systems [2, 5] is the measurement of the Hanle effect. The Hanle effect analyzes the decrease of the carrier spin polarization (typically via the circular polarization degree of photoluminescence) in a transverse magnetic field so that it also employs the clock defined by the Larmor precession. For relatively strong magnetic fields, for which the spin lifetime  $T_S$  is long compared to the time scale determined by the Larmor precession frequency  $\Omega_L$  ( $T_S \gg 1/\Omega_L$ ), the electron spins perform many revolutions during their lifetime [2]. Thus, the spin polarization along the direction of observation decreases with increasing transverse magnetic field. The Hanle curve describes this behavior. Its half-width at half maximum is given by  $B_{1/2} = \hbar/(\mu_B g_e T_S)$ , so the spin lifetime  $T_S$  can be obtained by measuring the Hanle curve, if the  $g$  factor is known [6–8].

Any Hanle effect-based method is based on the relax-

ation time approximation, in which the dynamics is described by one or a few exponents. It is a fair approximation, if the relaxation is caused, for example, by processes with short correlation times (Markovian processes) since these short correlation times lead to dynamic averaging over magnetic fields of different origin, acting on the electron. However, this approximation is violated for strongly localized electrons, when the dwell time of the electron on the donor exceeds the precession period of the electron spin in the hyperfine field of the nuclei. The width of the Hanle curve for donor-bound electron spins is determined by the relatively rapid precession in static nuclear fields [9], i.e. by the spin dephasing time  $T_2^*$ , and not by the longitudinal spin relaxation time  $T_1$ , which can be much longer than the precession period in the frozen nuclear field. Precession in static fields is reversible and to eliminate their effect the spin-echo method can be used [10]. However, this leads to a complication of experiments on the irreversible spin dynamics, designed to determine the  $T_1$  time.

We propose a different approach to measure the spin lifetime, which does not rely on the precession of the spins in a magnetic field applied in the Voigt geometry. This method uses an external clock instead of an internal one, namely the periodic polarization modulation of the exciting light with the modulation frequency  $f_m$ , and exploits the inertia of the spins: When switching the helicity of the light the steady-state value of the electron spin polarization is reached within a characteristic time  $T_S$ . At low modulation frequencies  $2\pi f_m \ll 1/T_S$ , compared to the time scale given by the spin lifetime, the electron spin polarization can overcome the spin inertia and reach its steady-state value for a particular laser polarization period. For high modulation frequencies  $2\pi f_m \geq 1/T_S$ , on the other hand, the electron spin polarization remains reduced since it cannot reach its steady-state value within a duty cycle with fixed circular polarization. The fall or rise of the spin polarization in dependence on the modulation frequency corresponds to the spin lifetime. With this method one can measure the spin lifetime in a weak magnetic field, when the dynamics of the average spin

is determined by relaxation processes in random fields that are not subject to dynamic averaging, i. e., when the method based on the Hanle effect cannot provide the time  $T_S$ .

A similar method was used by Akimov et al. [11, 12] to study the electron spin dynamics in epitaxial CdSe/ZnSe quantum dots. The method combines time- and polarization-resolved measurements of the emission from the trion singlet ground state with helicity modulation of the exciting light. However, the spin polarization was not measured in dependence of the modulation frequency by Akimov et al., so our method can be seen as an advancement. Fras et al. performed differential transmission measurements of InAs/GaAs quantum dots using the optical pump-probe technique [13]. Here, in addition to time-resolved measurements a technique called dark-bright time scanning spectroscopy was used, where the intensity of the exciting beam was modulated to measure in the frequency domain.

Fluorine doped ZnSe recently emerged as a promising material system in the field of solid-state quantum information technologies. So far indistinguishable single-photon-sources and optically controllable electron spin qubits were demonstrated [14–16]. Current efforts focus on gaining a detailed understanding of the electron and nuclear spin dynamics in this material.

Here, using the spin inertia method we investigate the spin dynamics of the strongly localized, donor-bound electrons in fluorine-doped ZnSe epilayers in a wide range of magnetic fields, temperatures, and pump densities. The paper is organized as follows. Section II provides details of the experimental techniques and studied samples. Section III describes the experimental results. Section IV is devoted to the theoretical consideration of the spin inertia effect. Modeling of the experimental data can be found in Section V. Discussion of the spin relaxation mechanisms is done in Section VI in combination with assessments on the applicability of the spin inertia method to various spin systems.

## II. EXPERIMENTAL DETAILS

We study two fluorine-doped ZnSe epilayers with different doping concentrations. The samples consist of three layers grown by molecular-beam epitaxy on (001)-oriented GaAs substrate. A thin ZnSe buffer layer reduces the strain induced by the II-VI on III-V heteroepitaxy. The ZnSe layer is followed by a 20-nm-thick  $\text{Zn}_{1-x}\text{Mg}_x\text{Se}$ ,  $x < 0.15$  barrier layer, which prevents carrier diffusion into the substrate. The fluorine-doped, 70-nm-thick ZnSe epilayer is grown on top of this barrier layer. Sample #1 has a fluorine concentration of about  $1 \times 10^{15} \text{ cm}^{-3}$ , while the doping of sample #2 is approximately three orders of magnitude higher ( $1 \times 10^{18} \text{ cm}^{-3}$ ). For the optical properties of these samples and for information on the electron spin dephasing we refer to Ref. [17].

The samples are placed in a vector magnet system consisting of three superconducting split-coils oriented orthogonally to each other [18]. It allows us to switch the

magnetic field from the Faraday geometry (magnetic field  $B_F$  parallel to the sample growth axis and the light wave vector) to the Voigt geometry (magnetic field  $B_V$  perpendicular to the sample growth axis and the light wave vector). The switching can be performed by using the respective pairs of split coils and does not require any changes of the optical alignment. Therefore we can measure in different magnetic field geometries with exactly the same adjustment of the pump and probe beams on a particular sample position. The measurements are performed at low temperatures with the samples either immersed in pumped liquid helium at  $T = 1.8 \text{ K}$  or cooled with controlled helium gas flow (up to 45 K). Photoluminescence (PL) spectra for sample characterization are excited using a continuous-wave (CW) laser with photon energy of 3.05 eV and detected with a Si-based charge-coupled device (CCD) camera attached to a 0.5-m spectrometer.

We use the pump-probe technique to study the electron spin dynamics by time-resolved Kerr rotation (TRKR). The electron spin coherence is created by circularly-polarized pump pulses of 1.5 ps duration (spectral width of about 1 meV) emitted by a mode-locked Ti:Sapphire laser operating at a repetition frequency of 75.7 MHz (repetition period  $T_R = 13.2 \text{ ns}$ ). The induced electron spin coherence is measured by linearly-polarized probe pulses of the same photon energy as the pump pulses (degenerate pump-probe scheme). A mechanical delay line is used to scan the time delay between the probe and pump pulses. The photon energy is tuned into resonance with the donor-bound heavy-hole exciton ( $D^0X\text{-HH}$ ) at about 2.80 eV. To obtain this photon energy a Beta-Barium Borate (BBO) crystal is used to double the frequency of the light generated by the Ti:Sapphire laser. The pump helicity is modulated between  $\sigma^+$  and  $\sigma^-$  polarization by an electro-optical modulator (EOM), so that on average the samples are equally exposed to left- and right-circularly-polarized pump pulses. The modulation frequency is varied between 10 kHz and 700 kHz. The photogenerated spin polarization results in a rotation of the polarization plane of the reflected, initially linear-polarized probe pulses due to the magneto-optical Kerr effect. The Kerr rotation (KR) angle is measured by a 10 MHz balanced photoreceiver with adjustable gain and bandwidth, connected to a lock-in amplifier. The pump density is varied in the range  $P_{\text{pump}} = 0.2 - 4.2 \text{ W/cm}^2$  and the probe density ( $P_{\text{probe}}$ ) is about one order of magnitude smaller than the pump density.

We use three different implementations of the pump-probe Kerr rotation method:

- (1) The time-resolved Kerr rotation configuration, where the Kerr rotation angle is measured in dependence of the time delay between the pump and probe pulses with the magnetic field applied in the Voigt geometry. In this case the Larmor precession of the electron spin polarization around the magnetic field axis results in a signal which is a periodic function of the time delay and whose amplitude decreases with increasing time delay. Using this configuration one can determine the  $g$  factor of the carriers and the inhomogeneous spin dephasing times  $T_2^*$  in the limit  $T_2^* < T_R$  [17].

(2) The resonant spin amplification (RSA) configuration [1, 19, 20] is used to determine  $T_2^*$  when this time is comparable to or greater than the laser repetition period  $T_R$ . Here the time delay between pump and probe is fixed at a small negative value ( $\Delta t \approx -20$  ps) and one measures the KR angle in dependence of the magnetic field applied in the Voigt geometry in the range from  $-20$  to  $+20$  mT. At certain magnetic fields the electrons spins precess in phase with the laser repetition frequency and one observes an increased Kerr rotation signal. Thus, the RSA signal consists of a symmetrical set of equidistant peaks, whose amplitude decreases with increasing magnetic field.

(3) In the polarization recovery (PR) configuration the electron spin polarization is detected as well at a small negative time delay. The KR signal is measured in dependence of the magnetic field applied in the Faraday geometry. The electron spin polarization, which is photogenerated along the magnetic field direction, does not exhibit Larmor precession then. Still it decreases by the nuclear hyperfine fields, if the external magnetic field is small compared to these fields. The effect of the hyperfine fields is suppressed with increasing external magnetic field. As a result, the electron spin polarization has its minimum at zero external magnetic field and increases with magnetic field. By varying the pump helicity modulation frequency one can measure the longitudinal spin relaxation time  $T_1$  of the electrons. We will mostly use this implementation to study the spin dynamics of the donor-bound electrons.

Note that the measurement of the KR signals at negative time delay, prior to the pump pulse, as done in the RSA and PR configurations greatly simplifies the interpretation of the signal origin. These signals can only arise from long-living spins, whose lifetime exceeds  $T_R = 13.2$  ns. This is typically much longer than the exciton recombination time, so that the measured signals can originate only from resident electrons, which are bound to donors at low temperatures.

In addition, we also perform pump-probe experiments using a CW pump and a pulsed probe. For these measurements a CW Ti:Sapphire laser with intra-cavity second harmonic generation is used as the pump, and the probe pulses are generated from the laser system described above. This configuration allows us to set the pump and the probe laser at different photon energies, i.e. to perform two-color nondegenerate pump-probe measurements. Thereby we measure the PR and the suppression of the KR signal in the Voigt geometry (the Hanle curve), to investigate possible influences of pulsed excitation on the spin relaxation.

### III. EXPERIMENTAL RESULTS

Figure 1 shows the PL spectra of the two studied samples, measured at zero magnetic field for a temperature of  $T = 1.8$  K. The spectrum of sample #1 exhibits the following emission lines: Donor-bound heavy-hole exciton ( $D^0X$ -HH) at 2.7970 – 2.7997 eV, free heavy-hole exciton (FX-HH) at 2.8045 eV, donor-bound light-hole exciton

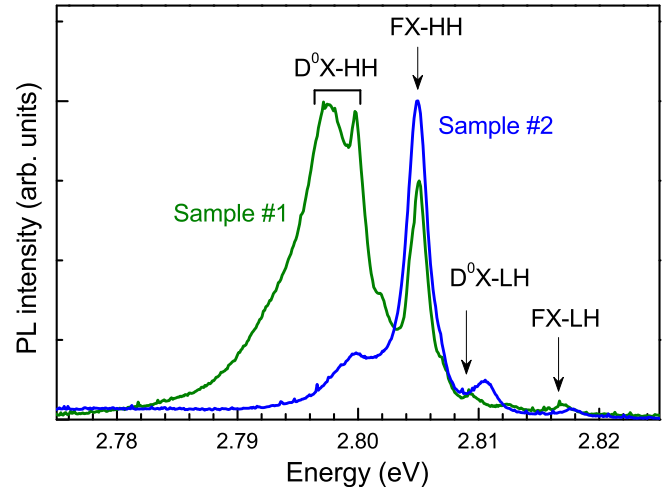


FIG. 1: (Color online) PL spectra of the fluorine-doped ZnSe epilayers #1 and #2 measured at  $B = 0$  T for  $T = 1.8$  K.

( $D^0X$ -LH) at 2.8092 eV and free light-hole exciton (FX-LH) at 2.8167 eV [17]. The strain induced by the II-VI on III-V heteroepitaxy lifts the light-hole and heavy-hole degeneracy for both structures [17]. The donor-related lines for the higher doped sample #2 exhibit a small blue-shift, compared to the same lines for sample #1.

Results of pump-probe measurements in all three experimental configurations are illustrated in Fig. 2 for sample #1. Results obtained with the TRKR and RSA configurations were considered in detail in Ref. [17] and are given here for illustration and comparison with the PR data. Furthermore, they provide important supplementary information on the donor-bound electron spins.

Figure 2(a) shows a time-resolved Kerr rotation signal measured at a temperature of  $T = 1.8$  K for resonant  $D^0X$ -HH excitation. A magnetic field of  $B_V = 0.42$  T is applied in the Voigt geometry and the observed oscillations reflect the Larmor precession of the electron spin polarization. Note that these oscillations are long-living and do not fully decay during the time interval  $T_R = 13.2$  ns between subsequent pump pulses, as can be seen from the considerable signal amplitude at negative time delays. The exciton lifetime in ZnSe is shorter than 250 ps [17], which allows us to conclude that the long-living TRKR signal originates from the coherent spin precession of the localized donor-bound electrons. The relatively large binding energy to these donors of 29 meV [21] provides strong electron localization and makes the spin coherence robust even at elevated temperatures up to 40 K [17]. We evaluate a  $g$  factor of the donor-bound electron of  $|g_e| = 1.13 \pm 0.02$  from the period of the signal oscillations. The same value of  $|g_e|$  is measured for sample #2.

Due to the long decay of the TRKR signal amplitude it is difficult to evaluate the electron spin dephasing time  $T_2^*$  by fitting the amplitude decay in these measurements. Instead we use the RSA technique for that purpose, for details see Ref. [17]. An example of a RSA signal is shown by the green line in Fig. 2(b). The analysis of the RSA peak width at  $T = 1.8$  K for low pump densities yields  $T_2^* = 33$  ns for the sample #1 and 8 ns for

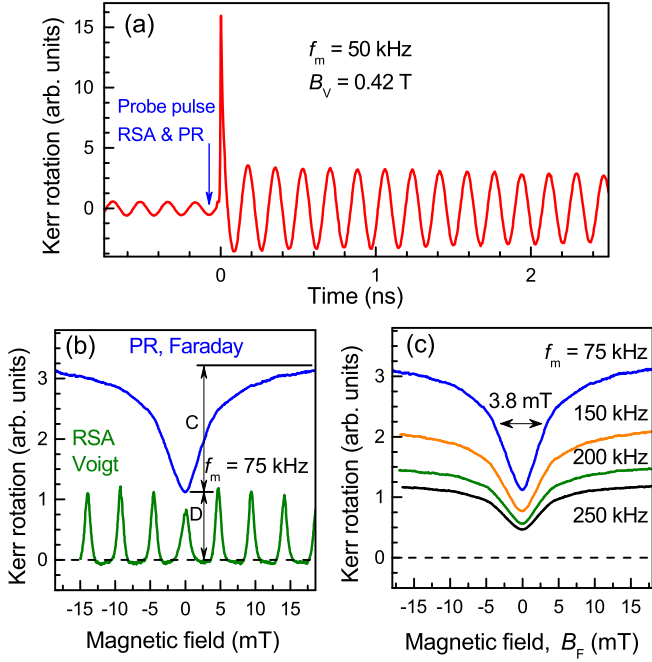


FIG. 2: (Color online) TRKR results for sample #1 measured for resonant  $D^0X$ -HH excitation (2.7986 eV) at  $T = 1.8$  K. (a) KR signal in dependence on the time delay at  $f_m = 50$  kHz and  $P_{\text{pump}} = 1.6$  W/cm $^2$ . The arrow marks the time delay at which the RSA and PR signals are detected. (b) PR and RSA signals measured at  $f_m = 75$  kHz. (c) PR signals measured at different modulation frequencies. In panels (b) and (c)  $P_{\text{pump}} = 0.5$  W/cm $^2$ .

the sample #2. The faster dephasing in the sample with higher fluorine concentration can be explained by the interaction between electron spins localized at neighboring donors [17].

The polarization recovery signal measured for the same experimental conditions as the RSA signal (only the magnetic field geometry is changed from Voigt to Faraday) is shown in Fig. 2(b) by the blue line. The PR curve has a minimum at zero magnetic field, increases with increasing  $B_F$  and saturates at fields exceeding 20 mT. Obviously, the polarization recovery is caused by suppression of the depolarization of the electron spin along the magnetic field direction. We tentatively relate the depolarization around zero field to the effect of the fluctuating nuclear hyperfine fields, more details will be given in the discussion below.

As shown in Figure 2(b), the amplitude of the zero RSA peak is a little smaller than the amplitude of the neighboring peaks. This may be due to the following factors: 1) A small, additional magnetic field component perpendicular to  $B_V$  can lead to a reduction of the zero RSA peak amplitude [18]. This component can occur if there is a small inclination (about  $1 - 2^\circ$ ) of the sample plane with respect to the  $\mathbf{k}$ -vector (either horizontally or vertically). 2) An additional nuclear field induced at  $B_V$  may also lead to a reduction or an increase of the amplitude of the zero RSA peak [22].

Figure 2(c) shows PR signals, measured for different pump helicity modulation frequencies,  $f_m$ , varied from

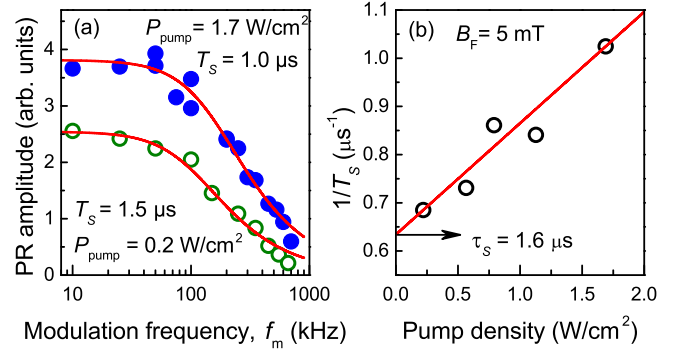


FIG. 3: (Color online) Spin dynamics measured for sample #1 with the PR technique at  $B_F = 5$  mT for  $T = 1.8$  K. (a) PR amplitude in dependence of  $f_m$  for two pump densities of 0.2 and 1.7 W/cm $^2$ . Red lines show the fits to the data based on our theoretical model (cf. Eq. (9)), which is used to determine the spin lifetime  $T_S$ . (b) Inverse spin lifetime  $1/T_S$  in dependence of the pump density. Red line is linear fit to the data, which is used to extrapolate the spin relaxation time  $\tau_S = 1.6$   $\mu$ s.

75 up to 250 kHz. The magnitude of the PR signal decreases for higher  $f_m$ , while the full width at half maximum (FWHM) of the dip around the zero magnetic field of about 3.8 mT and the overall shape of the PR curves remain the same. From these findings one can suggest that the inverse electron spin relaxation time falls in the examined frequency range.

To study this in more detail the PR amplitude in dependence of the modulation frequency is measured at  $B_F = 5$  mT for two pump densities. The PR amplitude for both pump densities, shown by the symbols in Fig. 3(a), remains constant for low modulation frequencies on the order of a few 10 kHz, while it rapidly decreases above 100 kHz. Model calculations shown by the red lines (details will be given in Secs. IV and V) allow us to evaluate the spin lifetime  $T_S = 1.5$   $\mu$ s for  $P_{\text{pump}} = 0.2$  W/cm $^2$  and  $T_S = 1.0$   $\mu$ s for  $P_{\text{pump}} = 1.7$  W/cm $^2$ . The spin lifetime in dependence of the pump density is plotted in Fig. 3(b). The decrease of the PR amplitude with increasing  $f_m$  is the key result of this study. In the following we present details of its change with varying magnetic field strength and temperature in order to obtain comprehensive information on the spin dynamics of the donor-bound electrons in ZnSe.

The blue circles in Fig. 4(a) illustrate the spin relaxation time  $\tau_S$ , determined with our model, in dependence of the magnetic field, varied from zero to 20 mT. The black line shows the corresponding PR signal at  $f_m = 75$  kHz. The spin relaxation time remains constant within the accuracy of our method in this  $B_F$  range. The PR signal in an extended magnetic field range up to 0.5 T is shown in Fig. 4(b). One sees that the signal is pretty much constant in the field range from 0.02 to 0.5 T. In this range its amplitude decreases by a factor of 15, when  $f_m$  is changed from 75 kHz to 400 kHz (note the multiplication factor of 5 in the figure). For higher fields we perform measurements each 0.5 T in the range 1.0-2.5 T. For each field four modulation frequencies are examined (see Fig. 4(c)). For all measured  $f_m$  the PR amplitude is

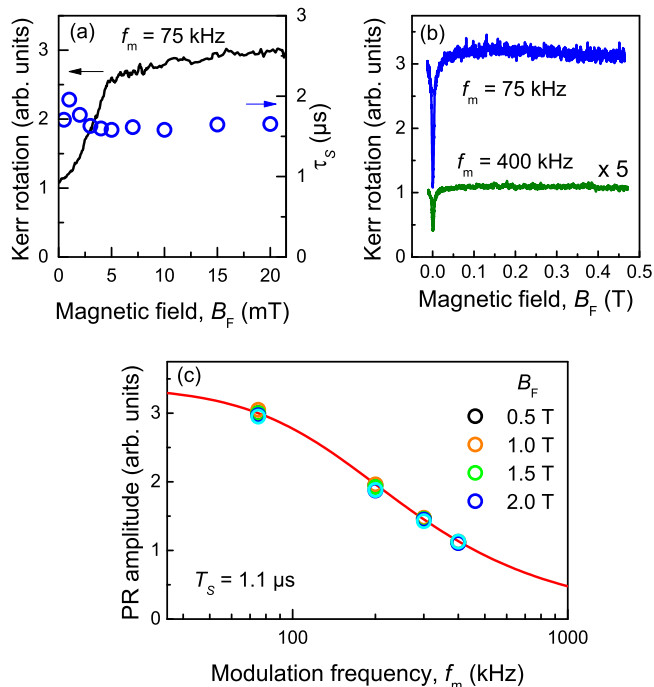


FIG. 4: (Color online) Results for sample #1 measured at  $T = 1.8$  K. (a) Blue circles give the spin relaxation time  $\tau_S$  in dependence of the magnetic field. Black line shows a typical PR signal.  $P_{\text{pump}} = 1.7$  W/cm $^2$ . (b) PR signals in dependence of  $B_F$  for  $f_m = 75$  kHz (blue line) and 400 kHz (green line).  $P_{\text{pump}} = 2.4$  W/cm $^2$ . (c) Modulation frequency dependence of the PR amplitude measured in different magnetic fields  $B_F$ .  $P_{\text{pump}} = 2.4$  W/cm $^2$ . Red line shows fit to the data according to Eq. (9) with the fit parameter  $T_S = 1.1$   $\mu$ s.

independent of the magnetic field strength. Its frequency dependence can be fitted with the same function shown by red line. From this fit we obtain  $T_S = 1.1$   $\mu$ s. An important experimental result of Fig. 4 is that the PR amplitude in dependence of  $B_F$  considerably increases from zero to 20 mT, but then remains constant in the range from 20 mT up to 2.5 T.

The shape of the PR amplitude as function of the modulation frequency is maintained in the temperature range from 1.8 up to 45 K, as illustrated by the experimental data presented in Fig. 5, where results for  $T = 1.8$ , 30 and 45 K are compared. The PR amplitude decreases slightly by less than 40% for elevated temperatures and has been normalized to  $T = 1.8$  K at 100 kHz. The shape of the frequency dependence remains almost the same evidencing that the spin dynamics of the donor-bound electrons does not change at  $T < 45$  K.

The spin relaxation mechanism of optically oriented carriers may depend on whether CW or pulsed photoexcitation is used. Excitation of spins systems with short pulses of picosecond duration may induce perturbations assisting the spin relaxation. This problem has been addressed in Ref. [23], where the coherent spin dynamics of resident electrons in n-doped CdTe/(Cd,Mg)Te quantum wells has been compared for CW and pulsed excitation. But in this case the in-plane localizing potential of about 1 meV for the resident electrons formed by monolayer well width fluctuations is weak compared with the

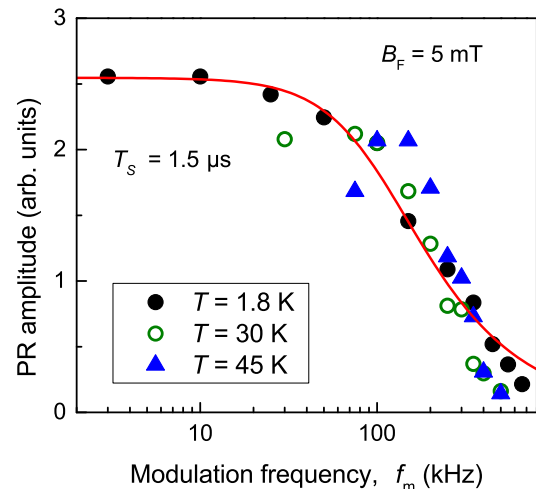


FIG. 5: (Color online) PR amplitude in dependence of the modulation frequency measured for sample #1 at three different temperatures. Data are normalized to each other at  $f_m = 100$  KHz.  $P_{\text{pump}} = 0.4$  W/cm $^2$ . Red line shows fit to the data at  $T = 1.8$  K according to Eq. (9) with the fit parameter  $T_S = 1.5$   $\mu$ s.

fluorine-donor binding energy of 29 meV in ZnSe.

The spin dynamics of the donor-bound electrons under CW pump measured for sample #2 is shown in Fig. 6(a). In this experiment the pump and the probe have different photon energies. The CW pump is resonant with the D $^0$ X-LH transition and the pulsed probe detects the electron polarization at the D $^0$ X-HH transition. Typically the energy relaxation between light-hole and heavy-hole exciton states is fast and does not lead to considerable losses in optical orientation. The magnetic field is applied in the Voigt geometry. A decrease of the spin polarization with increasing magnetic field is observed. This depolarization with increasing field can be assigned to the Hanle effect. The width of the Hanle curve is  $2B_{1/2} = 1.9$  mT. For comparison in Fig. 6(b) a PR curve for sample #2 is shown. It has a width of 3.8 mT, which is similar to the results for sample #1 (see Fig. 2(c)).

In the next two sections the chosen theoretical approach for describing the PR effect and its dependence on the pump helicity modulation frequency and the pump density is developed. The experimental data are fitted based on this model and the characteristic times for the electron spin dynamics are evaluated.

#### IV. THEORY

In n-type semiconductors the process of optical orientation results from the replacement of unpolarized resident electrons by photogenerated spin-oriented electrons [2]. The electrons loose their spin orientation due to spin relaxation with time  $\tau_S$ . Also their recombination with photogenerated holes will reduce the macroscopic electron spin polarization. As a result, the lifetime of the photogenerated electrons,  $\tau = n_0/G$ , depends on the rate of electron-hole generation  $G$ , and on the resident elec-

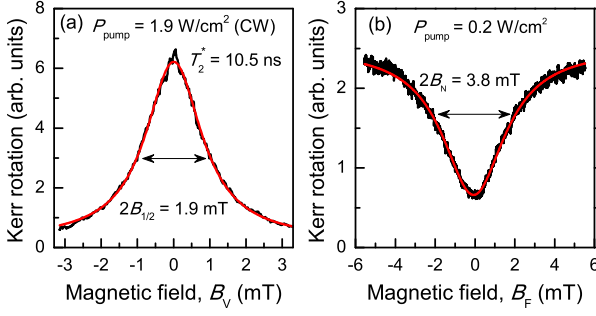


FIG. 6: (Color online) Spin dynamics of sample #2 measured by two different techniques at  $T = 1.8$  K and  $f_m = 50$  KHz. (a) Hanle curve induced by a CW pump resonant with the  $D^0X$ -LH transition (2.8092 eV) and detected with a pulsed probe at the  $D^0X$ -HH transition (2.7986 eV). Red line shows fit with a Lorentz curve (see Eq. (11) in Sec. V) giving  $B_{1/2} = 0.95$  mT corresponding to  $T_2^* = 10.5$  ns. (b) PR curve measured with pulsed pump and probe beams, both resonant with the  $D^0X$ -HH transition (2.7986 eV). Red line shows fit to the data using Eq. (12) with the fit parameter  $B_N = 1.9$  mT.

tron concentration  $n_0$ . The spin lifetime  $T_S$

$$1/T_S = 1/\tau + 1/\tau_S \quad (1)$$

determines the time until the steady-state spin polarization is reached by optical pumping.

In our experiment in the polarization recovery configuration the pump helicity is modulated, so that the spin polarization is switched between steady-state polarizations with opposite signs. On the one hand, if the modulation frequency is so small that the period with constant pump helicity is much longer than the spin lifetime ( $2\pi f_m \ll 1/T_S$ ), the average spin polarization seems to follow the pump polarization with negligible “inertia” effects (see Fig. 7). On the other hand, if the pump helicity modulation is so fast that the period with constant pump helicity is comparable to or shorter than the spin lifetime ( $2\pi f_m \geq 1/T_S$ ), the spin polarization cannot reach its steady-state value and the Kerr rotation signal is decreased significantly.

Let us consider the case when the electron spin polarization  $\mathbf{S}$  is generated along the  $z$ -axis, i.e. when the light wave vector of the pump laser is parallel to the  $z$ -axis ( $\mathbf{k} \parallel \mathbf{z}$ ). The amplitude of the Kerr rotation signal is proportional to  $S_z$ . The following kinetic equation describes the dynamics of the electron spin polarization [2]:

$$\frac{dS_z(t)}{dt} = \frac{S_i - S_z(t)}{\tau} - \frac{S_z(t)}{\tau_S}. \quad (2)$$

The initially generated spin polarization  $\mathbf{S}_i = (0, 0, S_i)$  depends on the laser polarization and optical selection rules. The first term in the right equation part describes the polarization injection ( $S_i/\tau$ ) and escape due to electron recombination ( $-S_z/\tau$ ) with time  $\tau$ , and the second term describes the spin relaxation with time  $\tau_S$ .

For constant circular polarization of the pump the stationary solution is:

$$S_z = S_0 = S_i \frac{\tau_S}{\tau_S + \tau} = S_i \frac{G\tau_S}{G\tau_S + n_0}. \quad (3)$$

For pump helicity modulation with a frequency  $f_m$  we have to solve the non-stationary Eq. (2). Combining Eqs. (1) and (2), we find

$$\frac{dS_z(t)}{dt} = \frac{S_0(t) - S_z(t)}{T_S}. \quad (4)$$

In our experiment  $S_0(t) = S_i(t) \frac{\tau_S}{\tau + \tau_S}$  is an alternating signal of rectangular pulses with a constant amplitude  $|S_0|$ , a duty cycle of 0.5 and the modulation frequency  $f_m$ .

In the PR experiment we measure the Kerr rotation signal, which is proportional to  $n_0 S_z$ . The spin polarization along the direction of observation  $S_z(t)$  is oscillating with the modulation frequency  $f_m$ . This means that we measure the following correlator:

$$L(f_m) = \langle S_z(t) \exp(i2\pi t/T_m) \rangle|_{T_m} = \int_0^{T_m} \frac{S_z(t) \exp(i2\pi t/T_m)}{T_m} dt. \quad (5)$$

The averaging is done over the pump modulation period  $T_m = 1/(2\pi f_m)$ . As a result, the task consists of two steps: (i) determine  $S_z(t)$  and (ii) calculate the correlator according to Eq. (5). The calculations show that the spin polarization along the direction of observation,  $S_z(t)$ , is a periodic function with the period  $T_m$  of the pump helicity modulation:

$$S_z(t) = |S_0| \left( 1 - \frac{2e^{-\frac{t}{T_S}}}{1 + e^{-\frac{T_m}{2T_S}}} \right), \quad (6)$$

in the half cycles in which  $S_0(t) = +|S_0|$ .

$$S_z(t) = |S_0| \left\{ -1 + 2 \left( e^{\frac{T_m}{2T_S}} - \frac{1}{1 + e^{-\frac{T_m}{2T_S}}} \right) e^{-\frac{t}{T_S}} \right\}, \quad (7)$$

in the half cycles in which  $S_0(t) = -|S_0|$ . Hence it is possible to determine the following correlator (5):

$$L(f_m) = -\frac{2n_0|S_0|}{\pi(i + 2\pi f_m T_S)}. \quad (8)$$

In the experiment the lock-in amplifier records the following signal:

$$|L(f_m)| = \frac{2}{\pi} \frac{n_0|S_0|}{\sqrt{1 + (2\pi f_m T_S)^2}}. \quad (9)$$

We use this expression to fit the PR amplitude in dependence of the modulation frequency, which allows us to evaluate  $T_S$ , as the only fitting parameter, by the spin inertia effect.

Figure 7 illustrates schematically the spin inertia effect and shows how the dependence of the correlator on the modulation frequency and the spin lifetime manifests itself in experiment. Figure 7(a) shows the time-dependent spin polarization along the direction of observation  $S_z(t)$  for two modulation periods. In the case of slow modulation compared to the spin lifetime (red line) the spin

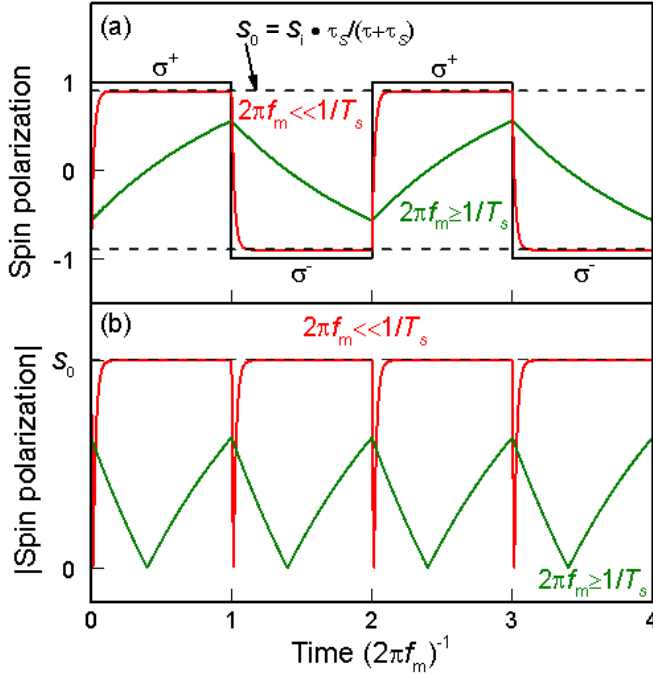


FIG. 7: (Color online) Illustration of the effect of electron spin inertia for pump helicity modulation with frequency  $f_m$ . The red and green lines show the limits of  $2\pi f_m \ll 1/T_S$  and  $2\pi f_m \geq 1/T_S$ , respectively. (a) Illustration of the spin polarization  $S_z$  along the direction of observation for two modulation periods: While in the first case the spin polarization follows the laser polarization without inertia and always reaches the steady state value  $S_0$  in a fixed laser polarization period, the spin polarization cannot reach  $S_0$  during such a period, when the modulation is fast compared to the time scale given by the spin lifetime  $T_S$ . (b) Modulus of the spin polarization  $|S_z(t)|$  for both limits. While in the first case ( $2\pi f_m \ll 1/T_S$ , red line)  $|S_z|$  is equal to  $|S_0|$  almost during the whole modulation period except for a small decrease, when the sign of the polarization is switched, the modulus of the spin polarization is strongly decreased during the whole modulation period for  $2\pi f_m \geq 1/T_S$ .

polarization follows the laser polarization without significant inertia and always reaches the steady state value  $|S_0|$  in a period of fixed laser polarization. However, the spin polarization cannot reach  $|S_0|$  during such a period, when the modulation occurs fast compared to the spin lifetime  $T_S$  (green line). Note that the time-averaged spin polarization is equal to zero in both cases. However, the lock-in amplifier records the signal, which is proportional to the time-averaged modulus  $|S_z|$  of the spin polarization (see Fig. 7(b)). For  $2\pi f_m \ll 1/T_S$  (red line) this time-averaged value is very close to  $|S_0|$ , while it is clearly smaller than  $|S_0|$  in the limit  $2\pi f_m \geq 1/T_S$ . We denote this impossibility of the spin polarization to follow the polarization of the exciting light for fast modulation compared to the spin lifetime as the spin inertia effect.

Investigation of the carriers spin dynamics by the spin inertia effect can be performed at zero as well as finite external magnetic fields. In magnetic field the evaluated spin relaxation time  $\tau_S$  corresponds to the longitudinal spin relaxation time  $T_1$ . It is also valid for sam-

ples in which the electron spins are affected by randomly oriented hyperfine fields from the nuclear spin fluctuations [9, 24], namely, when the spin dephasing time  $T_2^*$  caused by the nuclear fluctuations is considerably shorter than  $T_1$ . Note, that in this case the method based on the Hanle effect is limited to measurements of the  $T_2^*$  time, and not the  $T_1$  time, we discuss this in more detail in Sec. V.

For example, in our fluorine-doped ZnSe samples the donor-bound electrons are strongly localized. Thus, the dwell time of an electron on a donor is longer than the inhomogeneous dephasing time  $T_2^*$  of the ensemble of donor-bound electrons in the frozen hyperfine fields of the nuclei,  $\mathbf{B}_N$ . The components of the electron spin perpendicular to the hyperfine field decay during time  $T_2^*$ , while the spin polarization along the hyperfine field direction decays on a much longer time scale,  $T_1 \gg T_2^*$ . The effect of the fluctuating hyperfine fields can be taken into account in the model by adding the term  $\mathbf{\Omega}_N \times \mathbf{S}$  to Eq. (2) [9]:

$$\frac{d\mathbf{S}(t)}{dt} = \frac{\mathbf{S}_i - \mathbf{S}(t)}{\tau} - \frac{\mathbf{S}(t)}{\tau_S} + \mathbf{\Omega}_N \times \mathbf{S}. \quad (10)$$

Here  $\mathbf{\Omega}_N = \mu_B g_e \mathbf{B}_N / \hbar$ . The term  $\mathbf{\Omega}_N \times \mathbf{S}$  describes the precession of the spins in the frozen nuclear field with subsequent averaging over the Gaussian distribution of these fields [9]. Here one averages over an isotropic distribution of nuclear fields. Thus, the generated electron spin polarization decreases to one third of its initial value [9, 24]. Under these conditions the width of the Hanle curve is determined by the shortest characteristic time  $T_2^*$  [9]. However, the cutoff frequency on the spin inertia effect is still determined by the spin lifetime  $T_S$ , which originates from the  $T_1$  time. Due to the hyperfine fields the initial spin  $S_0$  in Eq. (9) depends on the sum of the external magnetic field and the hyperfine field averaged over the realizations of randomly oriented nuclear fields (see Ref. [24]).

## V. MODELING OF EXPERIMENTAL DATA

We interpret the decrease of the PR amplitude for increasing modulation frequency, shown in Figs. 2(c) and 3(a), as a decrease of the electron spin polarization due to the spin inertia effect. The red lines in Fig. 3(a) are fits to the data according to Eq. (9) for sample #1. From these fits we obtain spin lifetimes of  $T_S = 1.5$  and  $1.0 \mu\text{s}$  for low and high pump density, respectively. The pump density dependence of  $T_S$  is described by Eq. (1). Keeping in mind that  $\tau = n_0/G$ , one sees that for vanishing pump rates  $G$  the term  $1/\tau \rightarrow 0$  and  $T_S \rightarrow \tau_S$ . This gives us a way to measure the spin relaxation time  $\tau_S$ . Figure 3(b) shows the inverse spin lifetime  $1/T_S$  in dependence of the pump density. From extrapolates  $\tau_S = (1.6 \pm 0.1) \mu\text{s}$  for the data from sample #1 at  $T = 1.8$  K and  $B_F = 5$  mT. Performing measurements in the same experimental conditions for sample #2 we obtain  $\tau_S = (1.1 \pm 0.1) \mu\text{s}$ . In fact, the spin relaxation time of donor-bound electrons is weakly dependent on the donor concentration, which is not very surprising keeping in mind the strong localizing potential of the fluorine donors in ZnSe and that

the highest donor concentration we examine is approximately  $1 \times 10^{18} \text{ cm}^{-3}$ , i.e. the average distance between neighboring donors is about 10 nm.

The evaluated spin relaxation time  $\tau_S$  in dependence on the magnetic field is shown in Fig. 4(a) for the range of weak magnetic fields  $B_F < 20 \text{ mT}$ . It is constant in this field range at  $\tau_S = 1.6 \mu\text{s}$ . Note in particular that it is also constant below 5 mT where the electron spin polarization decreases considerably due to the fluctuating nuclear magnetic field as can be seen from the black line which shows the corresponding PR signal at  $f_m = 75 \text{ kHz}$ . Furthermore, the results presented in Figs. 4(a) and 4(c) let us conclude that the spin lifetime  $T_S$  and, correspondingly, the spin relaxation time  $\tau_S$  do not depend on  $B_F$  in the whole range from zero up to 2.5 T. Note, that this is a rather unexpected result as commonly the carrier spin relaxation time is sensitive to the application of magnetic fields. Figure 5 demonstrates another surprising observation, namely that the spin relaxation time does not depend on the temperature in the range from 1.8 to 45 K. We will discuss in Sec. VI possible spin relaxation mechanisms that can be responsible for this behavior.

Let us turn to the results recorded for CW pump, shown in Fig. 6(a). Here the spin polarization of donor-bound electrons is reduced in transverse magnetic field  $B_V$ , showing the known behavior for the Hanle effect. The common interpretation of the Hanle effect, when only an external magnetic field acts on the electron spin, is as follows. The external field  $B_V$  induces Larmor precession of the electron spins around the magnetic field direction ( $x$ -axis). The frequency of this precession is given by  $\Omega_L = \mu_B g_e B_V / \hbar$  [2]. For relatively strong magnetic fields, for which the spin lifetime  $T_S$  is long compared to the time scale determined by  $\Omega_L$ , the electron spins perform many revolutions during their lifetime. This precession reduces the projection of the spins on the initial direction ( $z$ -axis). The behavior is described by a Lorentz curve (the Hanle curve, see Eq. (50) in Ref. [2]).

$$S_z(B) = \frac{S_0}{1 + (B/B_{1/2})^2}, \quad (11)$$

Here  $B_{1/2} = \hbar / (\mu_B g_e T_S)$  is the characteristic field corresponding to the HWHM of the Hanle curve.

For localized electrons in semiconductors, the hyperfine fields of the nuclear spin fluctuations can also contribute to the Hanle curve. In the limit of a long dwell time of the electrons on the donors  $\Omega_N \tau_c \gg 1$  the half width of the Hanle curve will be controlled by the hyperfine field,  $B_{1/2} = \hbar / (\mu_B g_e T_2^*)$ , and the respective time is the spin dephasing time  $T_2^*$ . Here  $\tau_c$  is the correlation time of an electron and a donor. Using Eq. (11) to fit the experimental data by Fig. 6(a) we determine  $B_{1/2} = 0.95 \text{ mT}$ . In combination with  $|g_e| = 1.13$  for the donor-bound electron we obtain  $T_2^* = 10.5 \text{ ns}$ .

Alternatively, information on  $T_2^*$  can be obtained from the PR data shown in Fig. 6(b). The observed increase of the electron spin polarization for higher magnetic fields can be interpreted as a suppression of the influence of the nuclear spin fluctuations by the external magnetic field. The width of the observed dip of the PR curve can

be used as a direct measure of these fluctuations, which are characterized by an average hyperfine nuclear field  $B_N$  [17, 25]. The respective field dependence of the PR amplitude can be described by

$$\Theta_{\text{KR}} = \Theta_0 \left[ 1 - \frac{2/3}{1 + (B/B_N)^2} \right], \quad (12)$$

where  $\Theta_{\text{KR}}$  is the Kerr rotation angle, and  $\Theta_0$  is its value at zero magnetic field. The fit to the PR data with Eq. (12) shown in Fig. 6(b) yields  $B_N = 1.9 \text{ mT}$ . From this value one calculates  $T_2^*$  according to the following equation [25]:

$$T_2^* = 2\sqrt{3}\hbar / (\mu_B g_e B_N) \quad (13)$$

This calculation yields  $T_2^* = 18.3 \text{ ns}$ , which is in good agreement with the dephasing time evaluated from the Hanle curve.

Additional arguments for the validity of our interpretation come from the comparison of the RSA and PR signals measured under the same experimental conditions, see Fig. 2(b). There the PR amplitude (C) and the RSA peak amplitude at zero magnetic field (D) exhibit a ratio of about 2:1. This ratio is in good agreement with the conclusions of Ref. [24]. The Kerr rotation signal is a direct measure of the spin polarization along the direction of observation ( $z$ -axis). For weak or zero external magnetic fields the components of the nuclear field  $B_N$  oriented perpendicular to the direction of observation (i.e., the  $x$ - and  $y$ -components) depolarize the electron spins, while the components parallel or antiparallel to this axis ( $z$ -component) do not alter the spin polarization. Due to the isotropic nature of the nuclear fluctuations each of these three components of  $B_N$  has equal strength or probability, so that the spin polarization of the electron interacting with  $B_N$  is reduced to one third of its maximum value at zero external magnetic field [24, 25].

## VI. DISCUSSION

In this section we compare the characteristic times of the electron spin dynamics determined by the various techniques and discuss the spin relaxation mechanisms which can describe the measured properties of electron spins bound to fluorine donors in ZnSe. Comparing the results of the different techniques we find that  $\tau_S \gg T_2^*$ , i.e. the characteristic time determined from the Hanle curve  $T_2^*$  and the irreversible spin relaxation time  $\tau_S$  determined from the spin inertia method strongly differ. This can be explained by broadening of the Hanle curve by the nuclear spin fluctuations: The strongly localized, donor-bound electrons in the fluorine-doped ZnSe epilayers interact with the nuclear hyperfine field of the same nuclei for a long time ( $\tau_c \geq \hbar / (\mu_B g_e B_N)$ ). The resulting Larmor precession in the nuclear hyperfine field broadens the Hanle curve, so that the spin lifetime  $T_S$  obtained from the Hanle measurement is limited by this reversible effect and much shorter than the time for the irreversible spin relaxation  $\tau_S$  determined from the spin inertia method.

Every mechanism of irreversible spin relaxation can be interpreted as the effect of temporally fluctuating magnetic fields on the electron spin. Eq. (2) is valid in the case of short correlation times of the random magnetic field  $\tau_c \ll \tau_S$ , when dynamical averaging takes place. In a strong magnetic field the relaxation times of the longitudinal and transverse components  $T_1$  and  $T_2$  are different. The time  $T_1$  describes the decay of the spin component along the magnetic field. This time can depend considerably on the magnetic field, since the spin-flip requires the transfer of the energy  $\mu_B g_e B$  to the lattice. On the contrary, the time  $T_2$  describes the decoherence time, which is not related to energy transfer to the lattice. They become equal to each other  $T_1 = T_2 = \tau_S$  in a weak magnetic field [10]. The spin relaxation time  $\tau_S$  that we determine with the spin inertia method with the magnetic field applied in Faraday geometry is the  $T_1$  time.

For sufficiently strong longitudinal magnetic fields one would expect a dependence of the spin relaxation time on the magnetic field. However, we do not observe any dependence of  $\tau_S$  on the magnetic field from zero up to 2.5 T for the donor-bound electrons and only small variations within the accuracy of our method in the temperature range from 1.8 up to 45 K. This imposes severe restrictions on the fluctuating magnetic fields, which can be used to describe the spin relaxation process. Calculating the Zeeman splitting of the electron states at an external magnetic field of  $B = 2.5$  T we can deduce that the fluctuations of the random magnetic field describing the underlying relaxation mechanism must have a wide frequency range  $\mu_B g_e B / \hbar \approx (3 \text{ ps})^{-1}$ . Thus, the correlation time of the corresponding fluctuating field must be shorter than 3 ps.

The following, almost instantaneous processes can be considered: (i) scattering between free and donor-bound electrons (the exchange interaction between the electrons is responsible for the electron spin flip), (ii) jumping of electrons between different donors (hyperfine and spin-orbit interaction), (iii) scattering of phonons by donor-bound electrons (spin-orbit interaction), and (iv) charge fluctuations in the environment of the donors (spin-orbit interaction). All of them will be discussed in the following.

The process (i) is unlikely, because the localized states are excited resonantly and the donor ionization process should depend on temperature in the range from 30 to 50 K, which does not reflect the experimental observations.

The process (ii) can be provided by two mechanisms: Electron spin flip-flop transitions, which are induced by the scalar exchange interaction between electrons on neighboring donors, and electron jumps of donor-bound electrons to unoccupied donors. Calculations according to Ref. [28] for the parameters of the fluorine donor in ZnSe yield a jump time much longer than the estimated 3 ps. Thus, we discard option (ii) as a possible mechanism.

We also discard the process (iii), since we do not observe any temperature dependence of the spin relaxation time  $\tau_S$ , which we would expect for a phonon-mediated process.

The only possible mechanism left is the process (iv) - charge fluctuations in the environment of the donors,

which e.g. might occur during the 1.5 ps duration of the laser pulse illumination. We test this possibility by changing the pulsed pump beam to CW excitation. However, the determined spin relaxation time still does not depend on magnetic field or on temperature in the specified range. According to this check we can exclude a direct influence of the pulsed excitation on the spin relaxation. However, we cannot completely disregard any illumination induced mechanism, as charge fluctuations can be produced also by CW laser excitation in combination with carrier recombination during tens of picoseconds [16]. Still, there is no clear evidence for this so that we suggest that there may be a different, new mechanism, which determines the spin relaxation time in this system with strong electron localization.

## VII. CONCLUSIONS

We have suggested a method based on the spin inertia effect to measure the longitudinal spin relaxations time  $T_1$  of carriers. It exploits optical orientation of the carrier spins and their polarization recovery in magnetic field in the Faraday geometry, measured for different modulation frequencies of the laser helicity. The validity of this method is demonstrated for electrons bound to fluorine donors in ZnSe. An electron spin relaxation time of  $T_1 = 1.6 \mu\text{s}$  is measured for sample #1 in the temperature range 1.8–45 K. This time remains constant for magnetic fields varied from zero to 2.5 T and depends only weakly on the donor concentration. Measurements of the spin dephasing time  $T_2^* = 8 - 33$  ns by the RSA and Hanle techniques, and comparison of pulsed and continuous-wave excitation allow us to conclude that the spin relaxation of the donor-bound electrons is caused by perturbations that cover a broad spectral range. The question about the origin of this perturbation has remained open so far and needs further investigations.

The obvious advantage of the suggested polarization recovery technique based on the spin inertia effect is that it is suitable for measuring the longitudinal spin relaxation time  $T_1$  in the whole range of magnetic fields starting from zero field. Contributions of different spin relaxation mechanisms may be distinguished by their different onsets in the modulation frequency dependence. This distinction is possible when the generated carrier spin polarization is not fully destroyed by a faster relaxation mechanism. A requirement for the suggested technique is the finite optical orientation of carriers (at least of about few percent that can be comfortably detected). The photoinduced carrier spin polarization can be detected by various methods, e.g. by Kerr or Faraday rotation or by the circular polarization degree of photoluminescence. The main limitation of the technique comes from the condition that the pump helicity modulation period shall be tuned to a time shorter than the spin lifetime  $T_S$ . Therefore, the technique can be applied well for measuring long relaxation times, e.g. of resident carriers, but it is less suited for fast decaying excitons, for example, whose typical recombination time is shorter than a nanosecond, as it would require a modulation frequency

exceeding 1 GHz.

**Acknowledgements** This work has been supported by the Deutsche Forschungsgemeinschaft via Sonderforschungsbereich TRR 160, the Volkswagen Stiftung

(Project-No. 88360) and the Russian Science Foundation (Grant No. 14-42-00015). V.L. Korenev acknowledges financial support of the Deutsche Forschungsgemeinschaft within the Gerhard Mercator professorship program.

- 
- [1] D. D. Awschalom, D. Loss, and N. Samarth (eds.), *Semiconductor Spintronics and Quantum Computation* (Springer-Verlag, Berlin, 2002).
- [2] M. I. Dyakonov and V. I. Perel, Chap. 2, in *Optical Orientation*, eds. F. Meier and B. P. Zakharchenya, (North-Holland, Amsterdam, 1984).
- [3] W. Hanle, *Z. Phys.* **30**, 93 (1924).
- [4] C. Cohen-Tannoudji and A. Kastler, in *Progress in Optics* **5**, ed. E. Wolf (North-Holland, Amsterdam, 1966).
- [5] R. R. Parsons, *Phys. Rev. Lett.* **23**, 1132 (1969).
- [6] W. Happer, *Rev. Mod. Phys.* **44**, 169 (1972).
- [7] E. B. Aleksandrov, *Sov. Phys. Usp.* **15**, 436 (1973).
- [8] D. Budker, W. Gawlik, D. F. Kimball, S. M. Rochester, V. V. Yashchuk, and A. Weis, *Rev. Mod. Phys.* **74**, 1153 (2002).
- [9] R. I. Dzhiyev, V. L. Korenev, I. A. Merkulov, B. P. Zakharchenya, D. Gammon, Al. L. Efros, and D. S. Katzer, *Phys. Rev. Lett.* **88**, 256801 (2002).
- [10] A. Abragam, *The Principle of Nuclear Magnetism* (Oxford University Press, Oxford, 1961).
- [11] I. A. Akimov, D. H. Feng, and F. Henneberger, *Phys. Rev. Lett.* **97**, 056602 (2006).
- [12] I. A. Akimov, D. H. Feng and F. Henneberger, Chap. 4, in *Semiconductor Quantum Bits*, eds. F. Henneberger and O. Benson, (Pan Stanford Publishing, Singapore, 2009).
- [13] F. Fras, B. Eble, P. Desfonds, F. Bernardot, C. Testelin, M. Chamarro, A. Miard and A. Lemaitre, *Phys. Rev. B* **84**, 125431 (2011).
- [14] K. Sanaka, A. Pawlis, T. D. Ladd, D. J. Sleiter, K. Lischka, Y. Yamamoto, *Nano Letters* **12**, 4611 (2012).
- [15] D. J. Sleiter, K. Sanaka, M. Kim, K. Lischka, A. Pawlis, Y. Yamamoto, *Nano Letters* **13**, 116 (2013).
- [16] Y.M. Kim, D. Sleiter, K. Sanaka, D. Reuter, K. Lischka, Y. Yamamoto, A. Pawlis, *Curr. Appl. Phys.* **14**, 1234 (2014)
- [17] A. Greilich, A. Pawlis, F. Liu, O. A. Yugov, D. R. Yakovlev, K. Lischka, Y. Yamamoto, and M. Bayer, *Phys. Rev. B* **85**, 121303(R) (2012).
- [18] E. A. Zhukov, O. A. Yugov, I. A. Yugova, D. R. Yakovlev, G. Karczewski, T. Wojtowicz, J. Kossut, and M. Bayer, *Phys. Rev. B* **86**, 245314 (2012).
- [19] J. M. Kikkawa and D. D. Awschalom, *Phys. Rev. Lett.* **80**, 4313 (1998).
- [20] I. A. Yugova, M. M. Glazov, D. R. Yakovlev, A. A. Sokolova, and M. Bayer, *Phys. Rev. B* **85**, 125304 (2012).
- [21] J. L. Merz, H. Kukimoto, K. Nassau, and J. W. Shiever, *Phys. Rev. B* **6**, 545 (1972).
- [22] E. A. Zhukov, A. Greilich, D. R. Yakovlev, K. V. Kavokin, I. A. Yugova, O. A. Yugov, D. Suter, G. Karczewski, T. Wojtowicz, J. Kossut, V. V. Petrov, Y. K. Dolgikh, A. Pawlis, and M. Bayer, *Phys. Rev. B* **90**, 085311 (2014).
- [23] G. V. Astakhov, M. M. Glazov, D. R. Yakovlev, E. A. Zhukov, W. Ossau, L. W. Molenkamp, and M. Bayer, *Semicond. Sci. Technol.* **23**, 114001 (2008).
- [24] I. A. Merkulov, Al. L. Efros and M. Rosen, *Phys. Rev. B* **65**, 205309 (2002).
- [25] M. Y. Petrov, I. V. Ignatiev, S. V. Poltavtsev, A. Greilich, A. Bauschulte, D. R. Yakovlev, and M. Bayer, *Phys. Rev. B* **78**, 045315 (2008).
- [26] E. A. Zhukov, D. R. Yakovlev, M. Bayer, M. M. Glazov, E. L. Ivchenko, G. Karczewski, T. Wojtowicz, and J. Kossut, *Phys. Rev. B* **76**, 205310 (2007).
- [27] A. Greilich, R. Oulton, E.A. Zhukov, I. A. Yugova, D. R. Yakovlev, M. Bayer, A. Shabaev, Al. L. Efros, I. A. Merkulov, V. Stavarache, D. Reuter, and A. Wieck, *Phys. Rev. Lett.* **96**, 227401 (2006).
- [28] K. V. Kavokin, *Semicond. Sci. Technol.* **23**, 114009 (2008).